Computer Methods in Applied Mechanics and Engineering 425 (2024) 116945

Contents lists available at ScienceDirect

Comput. Methods Appl. Mech. Engrg.

journal homepage: www.elsevier.com/locate/cma

Multiharmonic multiscale modelling in 3-D nonlinear magnetoquasistatics: Composite material made of insulated particles

Janne Ruuskanen [a,c,*], Antoine Marteau [b], Innocent Niyonzima [b], Alexandre Halbach [c], Joonas Vesa [a], Gérard Meunier [b], Timo Tarhasaari [a], Paavo Rasilo [a]

[a] Tampere University, Electrical Engineering Unit, Tampere, FI-33720, Finland
[b] Univ. Grenoble Alpes, CNRS, Grenoble INP, G2Elab, Grenoble, F-38000, France
[c] Quanscient Oy, Tampere, FI-33100, Finland

ARTICLE INFO

Keywords:
Multiscale modelling
Multiharmonic method
Eddy current problems
Nonlinear magnetic materials
Mixed formulations

ABSTRACT

The use of the classical finite element method (FEM) to solve problems with magnetic composites leads to huge linear systems that are impossible to solve. Instead, homogenization and multiscale methods are often used with the composite material replaced by a homogeneous material with the homogenized constitutive law obtained by solving cell-problems representing the mesoscale material structure. For non-linear time-dependent problems, FEM is often used with a time-transient method (TTM) and the solution is obtained one time-step at a time. However, in cases where a steady-state solution is of interest, the multiharmonic method can be faster and more cost effective for the same accuracy of the time discretization. In addition, when solving magnetoquasistatic multiscale problems with TTM, the dynamic hysteresis in the homogenized fields can slow down or even impede the convergence of the macro-scale problem due to the possibly non-continuously differentiable homogenized material laws. This work presents a novel robust modelling approach for non-linear magnetoquasistatic problems combining multiharmonic method with the multiscale method.

1. Introduction

Composite materials (CM) play an important role in the field of electrical engineering [1]. However, due to their microscopic material structure, computational design of CM-based devices can be challenging with the classical finite element method (FEM) approach in several aspects. This work focuses on three particular challenges, posed by the numerical modelling of CM-based devices, and proposes a novel approach for improving the feasibility of simulating such devices in magnetoquasistatics with FEM. The three challenges are related to spatial, temporal and non-linear modelling of composite material.

The first challenge posed by the simulation of CM-based devices results from the multiscale nature of the composites. The classical FEM approach becomes infeasible due to the extremely dense mesh needed for the CM domains, but such FEM problems can be made tractable by the use of a multiscale method (MSM). In MSM, the composite material is homogenized, and the homogenized material properties are obtained by solving cell FEM-problems representing the composite material behaviour [2–5]. In the research field of computational electromagnetics, the multiscale methods have been used for example in [6–9].

* Corresponding author at: Tampere University, Electrical Engineering Unit, Tampere, FI-33720, Finland.
E-mail address: janne.ruuskanen@tuni.fi (J. Ruuskanen).

https://doi.org/10.1016/j.cma.2024.116945
Received 4 December 2023; Received in revised form 29 February 2024; Accepted 20 March 2024
Available online 26 March 2024

The second challenge is related to the time-domain resolution of eddy current problems. The usual approach is the time-transient method (TTM) where the time evolution of the electromagnetic fields is obtained by solving the problem one time-step at a time. However, especially in the case where the steady-state is of interest, TTM can require simulating several time-periods and a high number of time-steps in order to reach the steady-state. In the worst case, this method can be practically infeasible due to the long simulation time. For such time-periodic problems, the multiharmonic method (MHM) can be a better choice over TTM in terms of simulation time [10]. In MHM, the electromagnetic fields in the time-domain are represented by a truncated Fourier series where the field coefficients depend only on the spatial variable.

The third challenge is related to the resolution of FEM problems with non-linear material laws. The common approach uses the Newton–Raphson (NR) method which involves the linearization of the nonlinear problem and the resolution of the linearized problem using an iterative scheme. However, convergence issues have been observed especially for formulations that use concave material laws. To overcome this challenge, the work uses a mixed FEM formulation having convex constitutive relation for both electric and magnetic fields [11]. The resulting $\boldsymbol{BJ}$ conforming formulation uses the vector potentials $\boldsymbol{A}$ and $\boldsymbol{T}$ for the magnetic flux density $\boldsymbol{B}$ and the electric current density $\boldsymbol{J}$ respectively defined by $\boldsymbol{B} = \operatorname{curl} \boldsymbol{A}$ and $\boldsymbol{J} = \operatorname{curl} \boldsymbol{T}$.

An additional benefit, related to the second and the third challenge, that comes with using MHM in the multiscale modelling is the avoidance of the possible convergence issues with the Newton–Raphson method (NR) arising from the eddy-current effects. At high frequencies, the eddy currents can cause so-called dynamic hysteresis visible in the homogenized field relations in the macro-scale. Due to this effect, the macroscopic magnetic field strength can be non-continuously differentiable with respect to the macro-scale magnetic flux density as it will be highlighted later in Section 5. Consequently, challenges in solving the macro-scale problem with the NR-method can be encountered.

To overcome the three challenges, this work presents a novel FEM modelling approach for CM-based devices using a magneto-quasistatic formulation with robust non-linear convergence, and combines the multiscale method with the multiharmonic method. The novelty of this multiharmonic multiscale method (MMM) lies in the use of the already existing MHM method and the $\boldsymbol{BJ}$ mixed formulation in order to develop a novel multiscale method. In this work, its performance is demonstrated in the simulation of a CM-based device.

The article is outlined as follows. In Section 2 the MHM is discussed for the essential background information, andSection 3 covers the background for the multiscale method. Section 4 formulates the magnetoquasistatic FEM problem for the TTM, MHM and MMM. Their capabilities are compared in Section 5. Finally, conclusions are drawn in Section 6. The appendix details the derivation of the homogenized quantities for the MMM.

2. Multiharmonic method

In this section, the multiharmonic method is briefly introduced with the spatio-temporal dependency of the fields discretized using the Fourier basis for the time and the usual FEM basis for the space.

Let us consider a spatio-temporal dependent magnetic flux density field $\boldsymbol{B}$ expressed as

$$\boldsymbol{B}(\boldsymbol{x},t) \approx \sum_{k=0}^{N} \boldsymbol{B}_{\mathrm{s},k}(\boldsymbol{x}) \sin(k\omega_0 t) + \boldsymbol{B}_{\mathrm{c},k}(\boldsymbol{x}) \cos(k\omega_0 t). \tag{1}$$

The coefficients $\boldsymbol{B}_{\mathrm{s},k}$ and $\boldsymbol{B}_{\mathrm{c},k}$ are spatially dependent vector fields to be approximated by FEM basis functions [12,13]. The subscript s, k associates the field to the coefficient of $\sin(k\omega_0 t)$ and c, k associates the field to the coefficient of $\cos(k\omega_0 t)$. The index $k = 0, \dots, N$ defines the kth harmonic in the series. The fundamental angular frequency is $\omega_0 = 2\pi f_0$, where f_0 is the fundamental frequency. The time domain of interest is the period defined by $I_T = [0, T]$, where $T = \frac{1}{f_0}$. Moreover, the harmonic is odd when k is an odd number and even when k is an even number. In the simulations carried out in this work, the source for the problem will be driven at the fundamental frequency which is an odd frequency. Consequently, the multiharmonic solution consists only of the odd harmonics [12].

Furthermore, for later convenience (1) can be equivalently expressed as

$$\boldsymbol{B}(\boldsymbol{x},t) \approx \sum_{i=0}^{2N-1} \boldsymbol{B}_i(\boldsymbol{x}) \Theta_i(t), \tag{2}$$

where $\boldsymbol{B}_i(\boldsymbol{x})$ is the i^{th} spatial field and $\Theta_i(t)$ the corresponding temporal basis function in (1). All the multiharmonic fields can be expressed with the same expansion as $\boldsymbol{B}$. Especially, the multiharmonic magnetic field strength $\boldsymbol{H}$ is expressed as[1]

$$\boldsymbol{H}(\boldsymbol{x},t) \approx \sum_{k=0}^{N'} \boldsymbol{H}_{\mathrm{s},k}(\boldsymbol{B}(\boldsymbol{x},t)) \sin(k\omega_0 t) + \boldsymbol{H}_{\mathrm{c},k}(\boldsymbol{B}(\boldsymbol{x},t)) \cos(k\omega_0 t), \tag{3}$$

or equivalently as

$$\boldsymbol{H}(\boldsymbol{x},t) \approx \sum_{i=0}^{2N'-1} \boldsymbol{H}_i(\boldsymbol{B}(\boldsymbol{x},t)) \Theta_i(t). \tag{4}$$

[1] To note, $\boldsymbol{B}$ is expressed as in (1).

The variational formulation of the Ampere's law ($\mathrm{curl}\, \boldsymbol{H}(\boldsymbol{B}) = \boldsymbol{J}_\mathrm{s}$) with multiharmonic electromagnetic fields is derived as follows. If $\boldsymbol{H}(\boldsymbol{B})$ is a non-linear relation, it is first expressed as a linear approximation for the Newton–Raphson method as

$$\boldsymbol{H}(\boldsymbol{B}) \approx \boldsymbol{H}^0(\boldsymbol{B}^0) + \left.\frac{\mathrm{d}\boldsymbol{H}(\boldsymbol{B})}{\mathrm{d}\boldsymbol{B}}\right|_{\boldsymbol{B}=\boldsymbol{B}^0(\boldsymbol{x},t)} \cdot \left(\boldsymbol{B} - \boldsymbol{B}^0\right), \tag{5}$$

where $\boldsymbol{B}^0(\boldsymbol{x},t)$ is the known magnetic flux density in space and time at the current NR-iteration, and $\boldsymbol{B}$ is the yet unknown magnetic flux density to be solved [6,10]. Hence, $\mathrm{curl}\, \boldsymbol{H}(\boldsymbol{B}) = \boldsymbol{J}_\mathrm{s}$ becomes

$$\mathrm{curl}\left(\boldsymbol{H}^0 + \left.\frac{\mathrm{d}\boldsymbol{H}(\boldsymbol{B})}{\mathrm{d}\boldsymbol{B}}\right|_{\boldsymbol{B}=\boldsymbol{B}^0(\boldsymbol{x},t)} \cdot \left(\boldsymbol{B} - \boldsymbol{B}^0\right)\right) = \boldsymbol{J}_\mathrm{s}, \tag{6}$$

and the variational formulation in the space–time domain $\Omega \times I_T$ becomes: for $i = 0, 1, \ldots, 2N-1$, find $\boldsymbol{A}_i \in H_0(\mathrm{curl};\Omega)$ with an appropriate gauge such that the weak form

$$\begin{aligned}&\left(\left(\boldsymbol{H}^0 + \left.\frac{\mathrm{d}\boldsymbol{H}(\boldsymbol{B})}{\mathrm{d}\boldsymbol{B}}\right|_{\boldsymbol{B}=\boldsymbol{B}^0(\boldsymbol{x},t)} \cdot \left(\boldsymbol{B} - \boldsymbol{B}^0\right),\ \boldsymbol{B}'\right)_\Omega,\ \Theta'\right)_{I_T}\\ &- \left(\left(\boldsymbol{J}_\mathrm{s},\ \boldsymbol{A}'\right)_{\Omega_\mathrm{s}},\ \Theta'\right)_{I_T} = 0\end{aligned} \tag{7}$$

holds $\forall \boldsymbol{A}' \in H_0(\mathrm{curl};\Omega)$ and $\forall \Theta' \in L^2(I_T)$ with $\boldsymbol{B}_i = \mathrm{curl}\, \boldsymbol{A}_i$. The inner product in the time domain ($I_T = [0,T]$) is defined by

$$(f,\ g)_{I_T} = \frac{2}{T}\int_0^T f(t)\cdot g(t)\ \mathrm{d}t, \tag{8}$$

where f, g belong to an appropriate function space (e.g., the functions f and g belong to the space $L^2(I_T)$). The inner product in the space domain Ω is defined by

$$(\boldsymbol{F},\ \boldsymbol{G})_\Omega = \int_\Omega \boldsymbol{F}(\boldsymbol{x})\cdot\boldsymbol{G}(\boldsymbol{x})\ \mathrm{d}\Omega, \tag{9}$$

where $\boldsymbol{F}$ and $\boldsymbol{G}$ belong to an appropriate function space (e.g., the functions $\boldsymbol{F}$ and $\boldsymbol{G}$ belong to $\boldsymbol{L}_2(\Omega)$ and the test functions $\boldsymbol{A}'$ form a basis of $H_0(\mathrm{curl};\Omega)$. Note that in this work, the notation $\mathrm{curl}\, \boldsymbol{A}' = \boldsymbol{B}'$ is used.

The basis Θ' consists of all the $\sin(k\omega_0 t)$ and $\cos(k\omega_0 t)$ -functions, for all $k = 0...N$, and the basis $\boldsymbol{A}'$ consists of all the $\boldsymbol{A}'_{\mathrm{s},k}$ and $\boldsymbol{A}'_{\mathrm{c},k}$, where $k = 0...N$ that are test fields for their respective unknown fields $\boldsymbol{A}_{\mathrm{s},k}$ and $\boldsymbol{A}_{\mathrm{c},k}$ with the usual Ritz–Galerkin FEM basis. The linear system corresponding to (7) can be obtained by testing with respect to all the basis functions in $\Omega \times I_T$. For the upcoming variational formulations, the nested inner-products in space and time are denoted in short as $(\cdot\ ,\ \cdot)_{\Omega\times I_T}$

To complete the explanation of the weak formulation of (7) with MHM, let us further clarify the derivative term

$$\left.\frac{\mathrm{d}\boldsymbol{H}(\boldsymbol{B})}{\mathrm{d}\boldsymbol{B}}\right|_{\boldsymbol{B}=\boldsymbol{B}^0(\boldsymbol{x},t)}. \tag{10}$$

Assuming that one has the constitutive relation for $\boldsymbol{H}(\boldsymbol{B})$, and its derivative with respect to $\boldsymbol{B}$ in hand, then (10) and $\boldsymbol{H}(\boldsymbol{B}^0(\boldsymbol{x},t))$ are known everywhere in $\Omega \times I_T$ and the inner products in (7) can be computed via spatial and temporal discretizations [12,13].

3. Multiscale method

In this section, the multiscale method (MSM) is explained using the same modelling domain as the one used in the upcoming simulations of the paper. In this work, the focus is on the device shown in Fig. 1 where the CM is made of magnetic and electrically conducting balls.

In the multiscale method, the original problem is decomposed into two problems: the macro-scale problem and the meso-scale problems. In the macro-scale problem, the CM is modelled as homogenized material, as illustrated in the left image of Fig. 2. The material properties are obtained by solving meso-scale cell-problems (right image of Fig. 2) at the macro-scale integration points. Hence, the original CM domain is decomposed into a macro-scale and into a meso-scale cell problem solved with the macroscopic field sources at each macro-integration point of the CM domain.

3.1. Homogenizing mesoscopic quantities

In this work, the field quantities of interest to be homogenized to the macro-scale are the magnetic field strength $\boldsymbol{H}$, the electric power density p_el and the magnetic power density p_mc of the conducting ball. The homogenized magnetic field strength is needed for solving the macro-scale problem, and the power densities are computed only over the conducting magnetic domains (Ω_mc) in the meso-scale domain in order to compare the simulation results between the multiscale and the reference problems.

The homogenized magnetic field strength [14] can be expressed based on the cell-field $\boldsymbol{h}$ as

$$\boldsymbol{H} = \frac{1}{2d^2_\mathrm{meso}}\begin{bmatrix}\int_{\Gamma_y^+} h_x\ \mathrm{d}\Gamma + \int_{\Gamma_z^+} h_x\ \mathrm{d}\Gamma\\ \int_{\Gamma_x^+} h_y\ \mathrm{d}\Gamma + \int_{\Gamma_z^+} h_y\ \mathrm{d}\Gamma\\ \int_{\Gamma_x^+} h_z\ \mathrm{d}\Gamma + \int_{\Gamma_y^+} h_z\ \mathrm{d}\Gamma\end{bmatrix}, \tag{11}$$

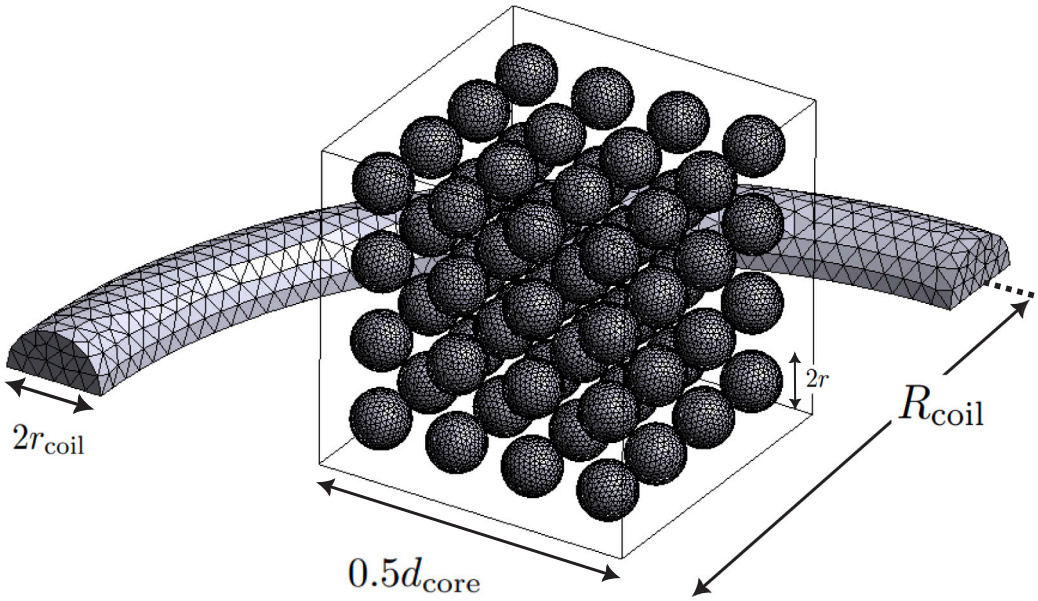

Fig. 1. The original modelling domain consists of a coil, and the composite material made of conducting nonlinear magnetic particles. Due to symmetry, in the simulations only the one-eighth of the full geometry, shown in the figure, is modelled.

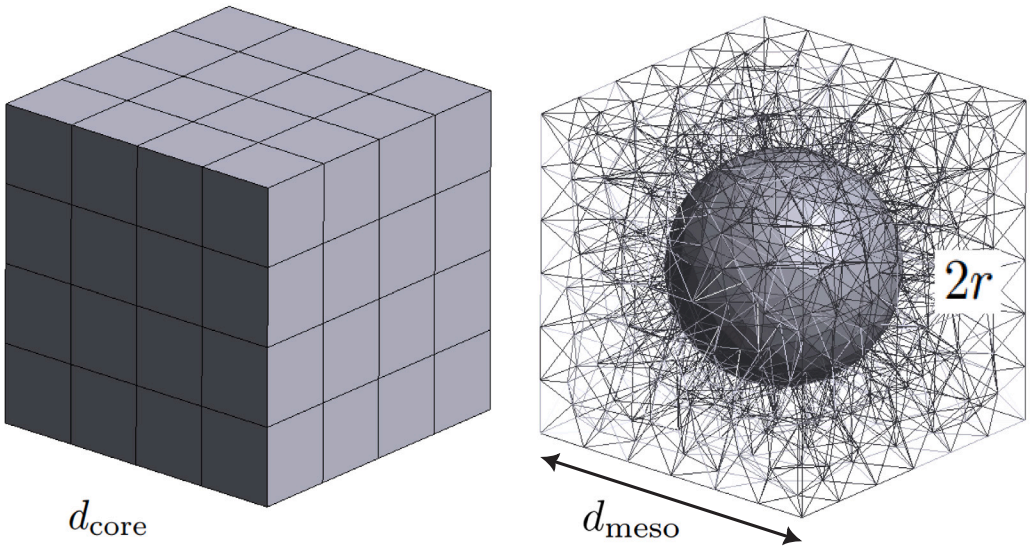

Fig. 2. Left: the homogenized macro-scale CM domain of the original problem. Right: the meso-scale cell representing the CM.

as detailed in Appendix A.1. Furthermore, as detailed in Appendix A.2, the macroscopic magnetic power density, of a conducting magnetic ball, is obtained as

$$p_{\mathrm{mc}}(t) = \frac{1}{|\Omega_{\mathrm{m}}|} \int_{\Omega_{\mathrm{mc}}} \partial_t \boldsymbol{b}(t) \cdot \boldsymbol{h}(t)\, \mathrm{d}\Omega. \tag{12}$$

The macroscopic eddy current loss density is obtained as

$$p_{\mathrm{el}}(t) = \frac{1}{|\Omega_{\mathrm{m}}|} \int_{\Omega_{\mathrm{mc}}} \boldsymbol{e}(t) \cdot \boldsymbol{j}(t)\, \mathrm{d}\Omega. \tag{13}$$

4. Magnetoquasistatic formulation

In this section, the formulation for the reference problem solved using the classical FEM with TTM and MHM, and the formulation for the multiharmonic multiscale problem are presented. Throughout the paper, the reference problem is referred to as TTM or MHM depending on whether it has been solved using TTM or MHM, and the multiscale problem is referred to as MMM.

The $\boldsymbol{BJ}$ conforming formulation based on the Maxwell's magnetoquasistatic model is used for both the reference problem and for the multiscale problem. The chosen formulation allows the use of convex constitutive relations in the formulation. Consequently, better convergence with the NR-method is obtained.

The following formulations are based on the topology depicted in Fig. 3, representing the device in Fig. 1 where the whole modelling domain $\Omega = \Omega_{\mathrm{nc}} \cup \Omega_{\mathrm{c}}$ and $\Omega_{\mathrm{s}} \subset \Omega_{\mathrm{nc}}$. Furthermore, the whole boundary of Ω is $\Gamma = \Gamma_{\mathrm{D}} \cup \Gamma_{\mathrm{N}}$. The domain Ω_{nc} refers to the nonconducting domain including the source domain Ω_{s} which is the coil with source current density. The domain Ω_{c} is the domain of conducting magnetic balls, and its boundary is denoted with Γ_{c}. The boundary of Ω ($\Gamma = \Gamma_{\mathrm{D}} \cup \Gamma_{\mathrm{N}}$) consists of the boundary Γ_{D} through which the normal component of the magnetic flux density is zero, and of the boundary Γ_{N} where the tangential field is required to be zero.

4.1. Reference problem formulation

The reference problem for the original modelling domain shown in Fig. 1 is derived based on the Maxwell's magnetoquasistatic model[2] [15]

$$\operatorname{curl} \boldsymbol{H}^{\epsilon} = \boldsymbol{J}^{\epsilon} + \boldsymbol{J}_{\mathrm{s}}, \tag{14}$$

$$\operatorname{curl} \boldsymbol{E}^{\epsilon} + \partial_t \boldsymbol{B}^{\epsilon} = \boldsymbol{0}, \tag{15}$$

$$\boldsymbol{n} \times \boldsymbol{T}^{\epsilon}\big|_{\Gamma_{\mathrm{c}}} = \boldsymbol{0}, \tag{16}$$

$$\boldsymbol{n} \times \boldsymbol{A}^{\epsilon}\big|_{\Gamma_{\mathrm{D}}} = \boldsymbol{0}, \tag{17}$$

where the magnetic field strength $\boldsymbol{H}^{\epsilon}$ is coupled with the magnetic flux density by the reluctivity ν as $\boldsymbol{H}^{\epsilon} = \boldsymbol{\mathcal{H}}(\boldsymbol{B}^{\epsilon}) = \nu(\boldsymbol{B}^{\epsilon})\boldsymbol{B}^{\epsilon}$, and the electric field strength $\boldsymbol{E}^{\epsilon}$ is coupled with the electric current density $\boldsymbol{J}^{\epsilon}$ by the resistivity ρ as $\boldsymbol{E}^{\epsilon} = \boldsymbol{\mathcal{E}}(\boldsymbol{J}^{\epsilon}) = \rho \boldsymbol{J}^{\epsilon}$. In this work, only linear $\boldsymbol{E}^{\epsilon} - \boldsymbol{J}^{\epsilon}$ relation is considered. The known source current density $\boldsymbol{J}_{\mathrm{s}}$ is imposed in the coil domain Ω_{s} to excite the problem. The vector potentials $\boldsymbol{A}^{\epsilon}$ and $\boldsymbol{T}^{\epsilon}$ are used for expressing $\boldsymbol{B}^{\epsilon}$ and $\boldsymbol{J}^{\epsilon}$ as $\boldsymbol{B}^{\epsilon} = \operatorname{curl} \boldsymbol{A}^{\epsilon}$ and $\boldsymbol{J}^{\epsilon} = \operatorname{curl} \boldsymbol{T}^{\epsilon}$ so that they satisfy $\operatorname{div} \boldsymbol{B}^{\epsilon} = 0$ and $\operatorname{div} \boldsymbol{J}^{\epsilon} = 0$. With TTM, the variational formulation for the reference problem becomes: for almost every $t \in I_T$, find $\boldsymbol{A}^{\epsilon}$ and $\boldsymbol{T}^{\epsilon}$ from appropriate function spaces such that:

$$\left(\boldsymbol{\mathcal{H}}(\boldsymbol{B}^{\epsilon}),\ \boldsymbol{B}^{\epsilon\prime}\right)_{\Omega} - \left(\boldsymbol{J}^{\epsilon},\ \boldsymbol{A}^{\epsilon\prime}\right)_{\Omega_{\mathrm{c}}} - \left(\boldsymbol{J}_{\mathrm{s}},\ \boldsymbol{A}^{\epsilon\prime}\right)_{\Omega_{\mathrm{s}}} = 0, \tag{18}$$

$$\left(\boldsymbol{\mathcal{E}}(\boldsymbol{J}^{\epsilon}),\ \boldsymbol{J}^{\epsilon\prime}\right)_{\Omega_{\mathrm{c}}} + \left(\partial_t \boldsymbol{B}^{\epsilon},\ \boldsymbol{T}^{\epsilon\prime}\right)_{\Omega_{\mathrm{c}}} = 0 \tag{19}$$

hold for all $\boldsymbol{A}^{\epsilon\prime}$ and $\boldsymbol{T}^{\epsilon\prime}$ with $\boldsymbol{B}^{\epsilon\prime} = \operatorname{curl} \boldsymbol{A}^{\epsilon\prime}$ and $\boldsymbol{J}^{\epsilon\prime} = \operatorname{curl} \boldsymbol{T}^{\epsilon\prime}$.

With MHM, the variational formulation for the reference problem becomes: find $\boldsymbol{A}^{\epsilon}$ and $\boldsymbol{T}^{\epsilon}$ from appropriate function spaces such that:

$$\left(\boldsymbol{\mathcal{H}}(\boldsymbol{B}^{\epsilon}),\ \boldsymbol{B}^{\epsilon\prime}\right)_{\Omega \times I_T} - \left(\boldsymbol{J}^{\epsilon},\ \boldsymbol{A}^{\epsilon\prime}\right)_{\Omega_{\mathrm{c}} \times I_T} - \left(\boldsymbol{J}_{\mathrm{s}},\ \boldsymbol{A}^{\epsilon\prime}\right)_{\Omega_{\mathrm{s}} \times I_T} = 0, \tag{20}$$

$$\left(\boldsymbol{\mathcal{E}}(\boldsymbol{J}^{\epsilon}),\ \boldsymbol{J}^{\epsilon\prime}\right)_{\Omega_{\mathrm{c}} \times I_T} + \left(\partial_t \boldsymbol{B}^{\epsilon},\ \boldsymbol{T}^{\epsilon\prime}\right)_{\Omega_{\mathrm{c}} \times I_T} = 0. \tag{21}$$

The unknown potentials are approximated with Whitney-1 elements and gauged with the spanning tree technique to ensure the uniqueness of the solution [16]. The whole domain Ω consists of the nonconducting part Ω_{nc} and of the conducting part Ω_{c}. Since $\boldsymbol{\mathcal{H}}(\boldsymbol{B}^{\epsilon})$ can be a non-linear relation, the term needs to be linearized as explained in Eq. (5) and the problem is solved iteratively with NR.

The electric and magnetic powers in Ω_{c} are computed in a post-processing step using respectively:

$$P_{\mathrm{el}}^{\epsilon}(t) = \int_{\Omega_{\mathrm{c}}} \boldsymbol{E}^{\epsilon}(t) \cdot \boldsymbol{J}^{\epsilon}(t)\, \mathrm{d}\Omega \tag{22}$$

[2] The fields are written with ϵ-superscripts to differentiate them from the macroscopic fields in the upcoming multiscale formulation.

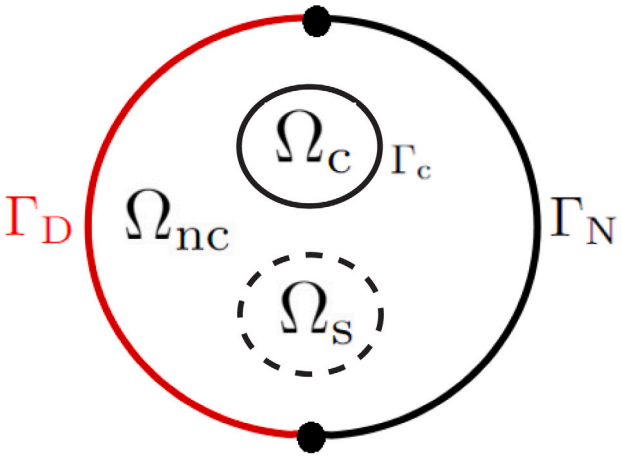

Fig. 3. Depiction of the modelling domain.

and

$$P^{\epsilon}_{\mathrm{mc}}(t) = \int_{\Omega_c} \partial_t \boldsymbol{B}^{\epsilon}(t) \cdot \boldsymbol{H}^{\epsilon}(t)\ \mathrm{d}\Omega \tag{23}$$

4.2. Multiscale problem formulation

In this section, the multiscale FEM problems for macro-scale and meso-scale are formulated.

4.2.1. Macro-scale formulation

This work focuses on the simulation of CM made of insulated conducting particles. Therefore, there is no electric currents in the macro-scale CM domain and the formulation becomes

$$\mathrm{curl}\ \boldsymbol{H}(\boldsymbol{B}) = \boldsymbol{J}_{\mathrm{s}}, \tag{24}$$

$$\boldsymbol{n} \times \boldsymbol{A}\big|_{\Gamma_{\mathrm{D}}} = \boldsymbol{0}, \tag{25}$$

and its variational formulation becomes: find $\boldsymbol{A}$ from an appropriate function space such that

$$\left(\boldsymbol{H}(\boldsymbol{B}),\ \boldsymbol{B}'\right)_{\Omega\times I_T} - \left(\boldsymbol{J}_{\mathrm{s}},\ \boldsymbol{A}'\right)_{\Omega_{\mathrm{s}}\times I_T} = 0, \tag{26}$$

which holds for all $\boldsymbol{A}'$ with $\boldsymbol{B}' = \mathrm{curl}\ \boldsymbol{A}'$. The field $\boldsymbol{H}$ in the homogenized CM domain is nonlinear with respect to $\boldsymbol{B}$, obtained by solving the cell-problem excited by the macroscale magnetic field $\boldsymbol{B}$ at the integration points of the CM domain. Elsewhere, $\boldsymbol{H}(\boldsymbol{B}) = \frac{1}{\mu_0}\boldsymbol{B}$.

The non-linear $\boldsymbol{H}(\boldsymbol{B})$ in the CM domain is linearized as follows. Let us denote the ith spatially unknown field of $\boldsymbol{B}$ by $\boldsymbol{B}_i$ as in (2). Then, similarly as in (5), the derivative of $\boldsymbol{H}$ with respect to $\boldsymbol{B}_i$ is

$$\boldsymbol{H}(\boldsymbol{B}) \approx \boldsymbol{H}(\boldsymbol{B}^0) + \sum_i \frac{\partial \boldsymbol{H}(\boldsymbol{B})}{\partial \boldsymbol{B}_i}\bigg|_{\boldsymbol{B}=\boldsymbol{B}^0} \cdot (\boldsymbol{B}_i - \boldsymbol{B}_i^0), \tag{27}$$

where the jth column of the tensor $\partial \boldsymbol{H}/\partial \boldsymbol{B}_i$ is approximated by means of finite difference as

$$\frac{\partial \boldsymbol{H}}{\partial_j \boldsymbol{B}_i}\bigg|_{\boldsymbol{B}=\boldsymbol{B}^0} \approx \frac{\boldsymbol{H}(\boldsymbol{B}^0 + \delta B \cdot \hat{\boldsymbol{v}}_j^i) - \boldsymbol{H}(\boldsymbol{B}^0)}{\delta B}, \tag{28}$$

where δB is the perturbation magnitude, and $\hat{\boldsymbol{v}}_j^i = \hat{\boldsymbol{v}}_j \Theta_i(t)$ addresses the perturbation to the jth spatial direction (x, y, z) on the ith term of $\boldsymbol{B}^0$. The spatial unit vector is denoted as $\hat{\boldsymbol{v}}_j$.

At the macro-scale, the electric and magnetic powers, as a function of time, are obtained respectively from the homogenized power densities, (12) and (13), by integration over the CM domain Ω_{CM} as

$$P_{\mathrm{el}}(t) = \int_{\Omega_{\mathrm{CM}}} p_{\mathrm{el}}(t)\ \mathrm{d}\Omega. \tag{29}$$

Table 1
Dimensions of the device geometry and the modelling domain.

d_{meso}	100 μm
r	$0.35d_{\text{meso}}$
r_{coil}	d_{meso}
d_{core}	$4d_{\text{meso}}$
R_{coil}	$3d_{\text{core}}$
R_{air}	$4d_{\text{core}}$

and

$$P_{\text{mc}}(t) = \int_{\Omega_{\text{CM}}} p_{\text{mc}}(t)\ \mathrm{d}\Omega. \tag{30}$$

4.2.2. Meso-scale formulation

The cell-problem is based on the cell shown on the right of Fig. 2. The cell Ω_{m}, having the boundary Γ_{m}, consists of the insulator domain Ω_{mi} and the conducting domain Ω_{mc}. Moreover, Γ_{mc} is the boundary of the conducting domain. The formulation of the cell problem is

$$\text{curl}\ \boldsymbol{h} = \boldsymbol{j}, \tag{31}$$

$$\text{curl}\ \boldsymbol{e} + \partial_t \boldsymbol{b} = \boldsymbol{0}, \tag{32}$$

$$\boldsymbol{n} \times \boldsymbol{a}_{\text{c}}\big|_{\Gamma_{\text{m}}}\ \text{periodic}, \tag{33}$$

$$\boldsymbol{n} \times \boldsymbol{t}_{\text{c}}\big|_{\Gamma_{\text{mc}}} = \boldsymbol{0}, \tag{34}$$

where $\boldsymbol{b} = \boldsymbol{B} + \boldsymbol{b}_{\text{c}}$, $\boldsymbol{j} = \boldsymbol{j}_{\text{c}}$, $\boldsymbol{b}_{\text{c}} = \text{curl}\ \boldsymbol{a}_{\text{c}}$ and $\boldsymbol{j}_{\text{c}} = \text{curl}\ \boldsymbol{t}_{\text{c}}$. The mesocale magnetic field strength $\boldsymbol{h}$ is coupled with the mesocale magnetic flux density $\boldsymbol{b}$ by the reluctivity ν as $\boldsymbol{h} = \boldsymbol{\mathcal{H}}(\boldsymbol{b}) = \nu(\boldsymbol{b})\boldsymbol{b}$, and the mesoscale electric field strength $\boldsymbol{e}$ is coupled with the mesoscale electric current density $\boldsymbol{j}$ by the resistivity ρ as $\boldsymbol{e} = \boldsymbol{\mathcal{E}}(\boldsymbol{j}) = \rho\boldsymbol{j}$. The vector potentials $\boldsymbol{a}_{\text{c}}$ and $\boldsymbol{t}_{\text{c}}$ are the unknown fields to be solved. They are approximated with Whitney-1 elements and gauged with the spanning tree technique. Furthermore, since $\boldsymbol{a}_{\text{c}}$ is spanned also on the periodic boundary of the cell, unlike $\boldsymbol{t}_{\text{c}}$, a periodic spanning tree was generated using Gmsh [17] to gauge $\boldsymbol{a}_{\text{c}}$. Furthermore, $\boldsymbol{a}_{\text{c}}$ was required to be periodic by translation on the opposite cell-faces. This enforces the homogenized magnetic flux density to be equal to the source $\boldsymbol{B}$. With MHM, the variational cell-formulation becomes: find $\boldsymbol{a}_{\text{c}}$ and $\boldsymbol{t}_{\text{c}}$ from appropriate function spaces such that[3]

$$\left(\boldsymbol{\mathcal{H}}(\boldsymbol{b}),\ \boldsymbol{b}'_{\text{c}}\right)_{\Omega_{\text{m}} \times I_T} - \left(\boldsymbol{j}_{\text{c}},\ \boldsymbol{a}'_{\text{c}}\right)_{\Omega_{\text{mc}} \times I_T} = 0, \tag{35}$$

$$\left(\boldsymbol{\mathcal{E}}(\boldsymbol{j}),\ \boldsymbol{j}'_{\text{c}}\right)_{\Omega_{\text{mc}} \times I_T} + \left(\partial_t \boldsymbol{b},\ \boldsymbol{t}'_{\text{c}}\right)_{\Omega_{\text{mc}} \times I_T} = 0, \tag{36}$$

hold for all test functions $\boldsymbol{a}'_{\text{c}}$ and $\boldsymbol{t}'_{\text{c}}$ with $\boldsymbol{b}'_{\text{c}} = \text{curl}\ \boldsymbol{a}'_{\text{c}}$ and $\boldsymbol{j}'_{\text{c}} = \text{curl}\ \boldsymbol{t}'_{\text{c}}$ Note that, the material relations in the cell are given by analytical relations. The problem is then solved similarly as the reference problem described in Section 4.1, i.e., in Ω_{mc} $\boldsymbol{h}(\boldsymbol{b})$ is non-linear and needs to be linearized for the NR method. In the insulator, the linear relation is $\boldsymbol{h}(\boldsymbol{b}) = \frac{1}{\mu_0}\boldsymbol{b}$.

5. Results

In this section, the predictive capabilities of the developed simulation approach (MMM) is compared with the reference problem solved with using the time-transient method TTM and the multiharmonic method MHM. The implementations were programmed using the C++ FEM library Sparselizard [18], and the simulations were carried out using the supercomputers of Finnish IT Center for Science. Gmsh [17] was used for creating modelling geometries, spanning trees and generating modelling meshes. Furthermore Gmsh was used for the visualization of the solved electromagnetic fields.

5.1. Problem set-up

The modelling domain and the mesh are shown in Fig. 1. Using symmetry, the domain presents one-eighth of the actual geometry. Hence, the upcoming results are calculated only for the modelling domain shown in the figure. The problem is excited by applying a sinusoidal current density in the coil with an amplitude of 30 GA/m^2 at the frequency of 100 kHz. The dimensions of the domain are detailed in Table 1 and their meanings are depicted in Fig. 1, except for R_{air} which is the radius of the external boundary of the modelling domain.

[3] Note that, $\boldsymbol{b}'_{\text{c}} = \text{curl}\ \boldsymbol{a}'_{\text{c}}$ and $\boldsymbol{j}'_{\text{c}} = \text{curl}\ \boldsymbol{t}'_{\text{c}}$.

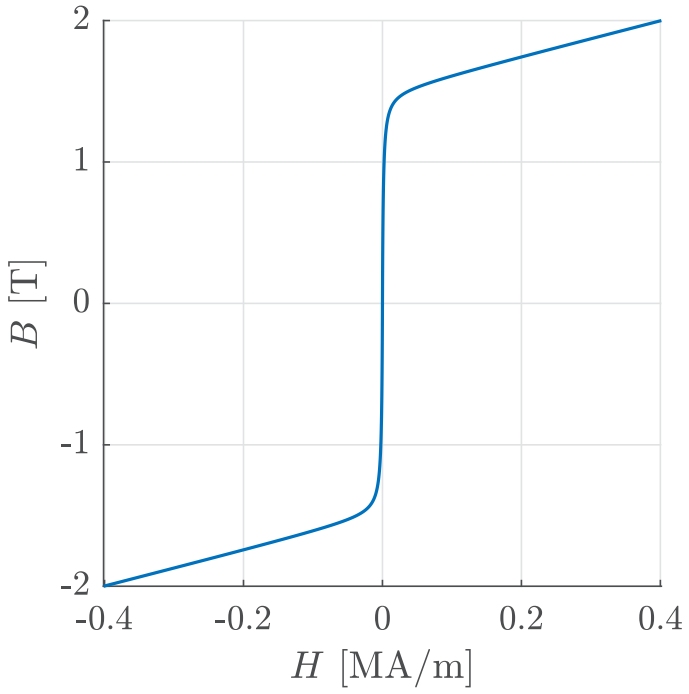

Fig. 4. The constitutive relation for the magnetic field in the CM particles.

Table 2
Maximum value of $||\boldsymbol{b}||$ at different harmonics.

k	1	3	5	7	9	11
$\max\|\|\boldsymbol{b}_k\|\|$	1.95	0.36	0.22	0.13	0.09	0.03
%	100	18.6	11.2	6.8	4.5	1.6

The particle material properties are as follows. The permeability in the particles are modelled according to the anhysteretic Fröhlich–Kennelly law [19]

$$\boldsymbol{B} = \mu(\boldsymbol{H})\boldsymbol{H}, \tag{37}$$

where

$$\mu(\boldsymbol{H}) = \mu_0 + \frac{\alpha}{B_\mathrm{s} + \beta\|\boldsymbol{H}\|}, \tag{38}$$

$B_\mathrm{s} = 1.5$ T, $\beta = \mu_0(\mu_\mathrm{r} - 1)$, $\alpha = \beta B_\mathrm{s}$ and $\mu_\mathrm{r} = 1000$. For the formulations used in this paper, the law was inverted to obtain $\boldsymbol{\mathcal{H}}(\boldsymbol{B}) = \nu(\boldsymbol{B})\boldsymbol{B}$. This material relation is shown in Fig. 4. Furthermore, for the electrical conductivity of the particles, constant $\sigma = 10$ MS/m is used, and for the non-conducting materials $\mu = \mu_0$ and $\sigma = 0$ S/m was used.

5.2. Stand-alone cell

Before solving the actual multiscale problem, the behaviour of the cell, representing the CM (right of image Fig. 2), was investigated when excited by a homogeneous $\boldsymbol{B}(t) = B_\mathrm{a}\sin(2\pi f_0 t)\cdot\hat{\boldsymbol{v}}_y$ in the y-direction where $B_\mathrm{a} = 0.8$ T and $f_0 = 100$ kHz.

Table 2 shows the maximum value of $\|\boldsymbol{b}\|$ at different harmonics, calculated as

$$\max\ \|\boldsymbol{b}_k\| = \max\ \sqrt{\boldsymbol{b}_{\mathrm{s},k}\cdot\boldsymbol{b}_{\mathrm{s},k} + \boldsymbol{b}_{\mathrm{c},k}\cdot\boldsymbol{b}_{\mathrm{c},k}}, \tag{39}$$

where $\boldsymbol{b}$ is expressed as (1). The row with the % denotes $\max\|\boldsymbol{b}_k\|$ normalized with $\max\|\boldsymbol{b}_1\|$. Based on this information, harmonics up to 7 will be used in the upcoming simulations.

Table 3 shows the norm of the homogenized magnetic field strength $\boldsymbol{H}$ for different harmonics, calculated as

$$\|\boldsymbol{H}_k\| = \sqrt{\boldsymbol{H}_{\mathrm{s},k}\cdot\boldsymbol{H}_{\mathrm{s},k} + \boldsymbol{H}_{\mathrm{c},k}\cdot\boldsymbol{H}_{\mathrm{c},k}}, \tag{40}$$

where $\boldsymbol{H}$ is expressed as (3).

Table 3
The norm of the different harmonics of the homogenized magnetic field strength.

k	1	3	5	7
$\|\|\boldsymbol{H}_k\|\|$	415 846	14 163	5434	223
%	100	3.4	1.3	0.05

Table 4
Homogenized magnetic and electric power density from the conducting ball domain at different harmonics.

k	$\|\|p_{\mathrm{mc},k}\|\|$ [GW/m^3]	%	$\|\|p_{\mathrm{el},k}\|\|$ [GW/m^3]	%
0	0	0	0.1175	81.8
2	1.3590	100.0	0.1435	100.0
4	1.1490	84.6	0.0622	43.3
6	0.4402	32.4	0.0414	28.9
8	0.0441	3.2	0.0096	6.7
10	0.1878	13.8	0.0034	2.4
12	0.1216	8.9	0.0011	0.8
14	0.0202	1.5	0.0001	0.1
16	0.0232	1.7	0	0
18	0.0188	1.4	0	0
20	0.0037	0.3	0	0

According to the results, it is sufficient to use the same harmonics for $\boldsymbol{H}$ as used for the cell fields. Based on this, in the upcoming simulations the macroscopic $\boldsymbol{B}$ will be approximated by default with harmonics 1 and 3. $\boldsymbol{H}$ will be approximated with the same harmonics as the cell-fields, i.e., odd harmonics from 1 to 7.

Table 4 shows the harmonic content of p_{mc} of (12) and p_{el} of (13), expressed using the Fourier series, for $k = 0, \dots, 20$, as

$$p_{\mathrm{mc}}(t) = \sum_{k=0}^{20} p_{\mathrm{mc,s},k} \sin(k\omega_0 t) + p_{\mathrm{mc,c},k} \cos(k\omega_0 t) \tag{41}$$

$$p_{\mathrm{el}}(t) = \sum_{k=0}^{20} p_{\mathrm{el,s},k} \sin(k\omega_0 t) + p_{\mathrm{el,c},k} \cos(k\omega_0 t). \tag{42}$$

The coefficients can be computed with the inner product (8) as

$$p_{\mathrm{mc,s},k} = \left(p_{\mathrm{mc}}(t),\ \sin(k\omega_0 t)\right)_{I_T} \tag{43}$$

$$p_{\mathrm{mc,c},k} = \left(p_{\mathrm{mc}}(t),\ \cos(k\omega_0 t)\right)_{I_T} \tag{44}$$

$$p_{\mathrm{el,s},k} = \left(p_{\mathrm{el}}(t),\ \sin(k\omega_0 t)\right)_{I_T} \tag{45}$$

$$p_{\mathrm{el,c},k} = \left(p_{\mathrm{el}}(t),\ \cos(k\omega_0 t)\right)_{I_T}. \tag{46}$$

Moreover, the norms of the fields at different harmonics are measured as

$$\|p_{\mathrm{mc,k}}\| = \sqrt{p_{\mathrm{mc,s},k}^2 + p_{\mathrm{mc,c},k}^2} \tag{47}$$

$$\|p_{\mathrm{el,k}}\| = \sqrt{p_{\mathrm{el,s},k}^2 + p_{\mathrm{el,c},k}^2}. \tag{48}$$

This investigation shows how many harmonics should be considered when homogenizing the power densities from the cell to the macro-scale. Based on the results, for the rest of the paper, a modelling decision is made to take into account even harmonics from 0 to 14 in the homogenized power densities.

The left image of Fig. 5 shows the homogenized magnetic field strength with respect to the source as a function of time over one period of excitation. It can be observed that the homogenized relation is only slightly non-linear even though the particle is highly saturated. On the right of the figure, the effect of the induced eddy currents in the cell particle on the $\boldsymbol{H}(\boldsymbol{B})$ relation is shown. This manifests itself in the dynamic hysteresis. If the multiscale problem was solved using a time-transient method, convergence challenges could be encountered with the NR-method due to the non-continuous derivative of $\boldsymbol{H}$ with respect to $\boldsymbol{B}$. To illustrate the behaviour of the electromagnetic fields in the cell, $\boldsymbol{b}$ and $\boldsymbol{j}$ are shown in Fig. 6 and Fig. 7, respectively.

5.3. Modelling magnetic composite material core

Finally, the performance of MMM is tested in the simulation of a magnetic composite material core device. The simulation problem is defined in Section 5.1. The strategy is to first obtain the reference solution and then compare with that the results given by MMM.

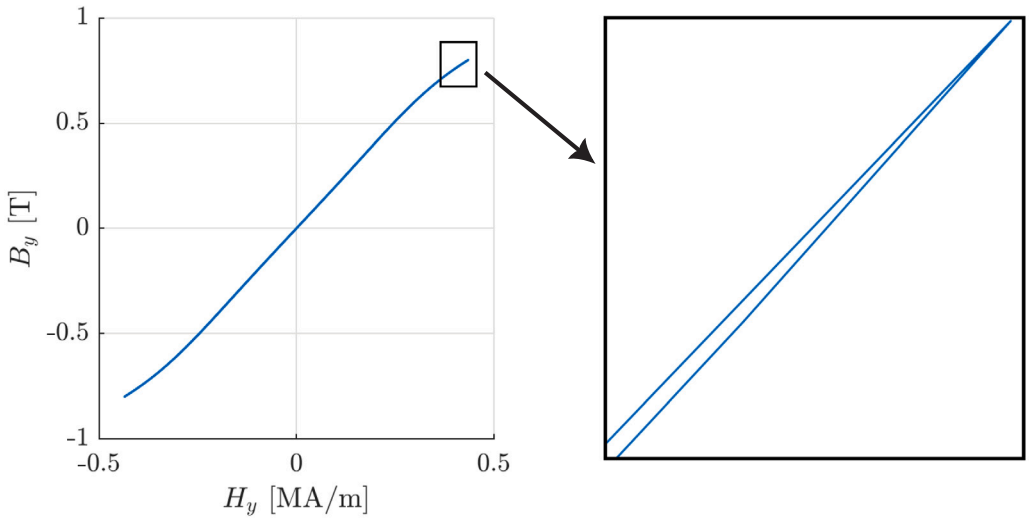

Fig. 5. The homogenized $\boldsymbol{B} - \boldsymbol{H}$ relation (left) has dynamic hysteresis due to the induced eddy currents in the particle of the cell as shown in the close-up figure on the right.

Table 5
The homogenized eddy current losses and magnetic power as a function of the number of macro-scale (odd) harmonics.

#harmonics	1	2	3	4
Simulation time [min]	34	57	85	119
avg(P_{el}) [mW]	5.29	5.31	5.32	5.31
Δ_{el} [%]	1.96	1.73	0.93	0.59
avg($\lvert P_{\mathrm{mc}} \rvert$) [mW]	17.98	17.22	16.89	16.80
Δ_{mc} [%]	10.1	5.02	2.17	1.66

5.3.1. Reference solutions

In order to compare the predictive capabilities and the performance of the MMM, the reference problem is first solved (see Section 4.1) with TTM and MHM. The TTM simulation of the reference problem was solved using the implicit Euler with a constant time-step. Only the first period of excitation was simulated with 250 time-steps, and the simulation time was 50 h. The MHM simulation of the reference problem was solved with MHM using harmonics {1,3,5,7} for $\boldsymbol{A}^{\epsilon}$ and $\boldsymbol{T}^{\epsilon}$. The simulation time was 10 h. The trapezoidal rule with 50 evenly spaced samples for the time-period were used for solving the inner-products (8) in I_T.[4]

Fig. 8 shows the electric power (22) and the magnetic power (23) during the first period of excitation, predicted by TTM and MHM. The results show good agreement between the two methods already after the first quarter of the first period. Note that MHM predicts the steady-state solution while TTM models the device behaviour including the initial transient phase. Due to the long simulation time with TTM, only the first period was simulated. Therefore, the steady-state may not have been reached yet. However, a modelling assumption is made that the TTM solution is in the steady-state after the first half of the time-period.

The simulation results for TTM and MHM are as follows. The relative difference, between TTM and MHM, in the average steady-state $P^{\epsilon}_{\mathrm{el}}$ was 0.02%, where TTM predicted 5.284 mW, and MHM predicted 5.285 mW. The relative difference in the average steady-state $P^{\epsilon}_{\mathrm{mc}}$ was 0.67%, where TTM predicted 16.64 mW and MHM predicted 16.52 mW. To note, from hereon the solution of MHM is used as the reference solution, and the upcoming simulation results obtained with MMM are compared with the results given by MHM.

5.3.2. Multiscale solutions

Next, MMM is deployed to simulate the behaviour of the CM device. As the starting point, 4^3 elements are used in the homogenized CM domain. Hence, the size of the macro-scale element corresponds with the size of the cell. A total of 64 CPUs were used to parallelize the computation of the homogenized field quantities associated with each macro-element. Harmonics {1,3,5,7} were used for the unknown vector potentials in the cell-problem. Table 5 shows the effect of the number of harmonics, used for the macro-scale unknown vector potentials, on the solution accuracy with respect to the reference solution obtained with MHM. In the

[4] The same number of samples are used for the time-domain inner-products throughout this work.

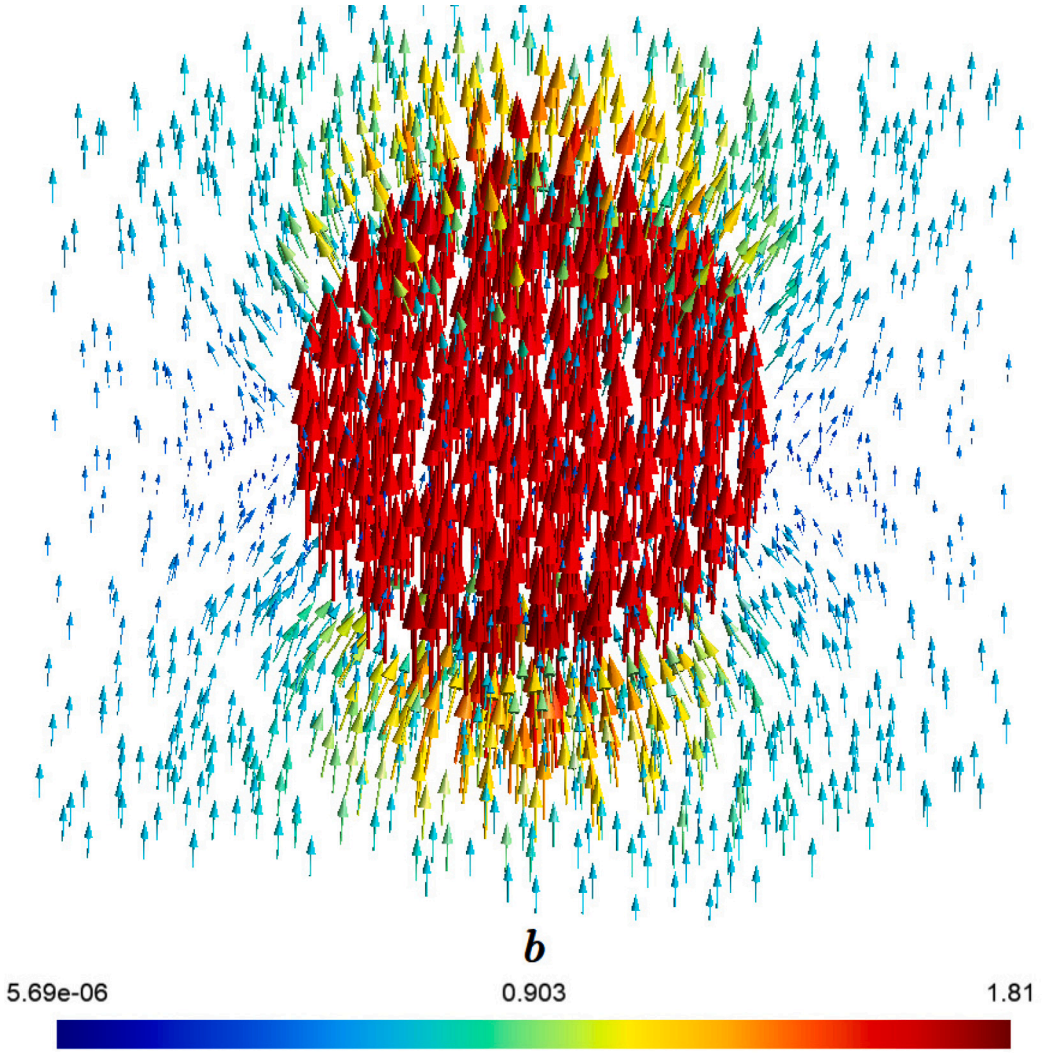

Fig. 6. Magnetic flux density in the cell when sourced with y-directional $B(t) = 0.8 \cdot \sin(\omega t)$ [T] at the frequency of 100 kHz.

table, the relative differences in the electric and magnetic powers are computed, respectively, as

$$\Delta_{\mathrm{el}} = \frac{\int_{I_T} |P^{\varepsilon}_{\mathrm{el}}(t) - P_{\mathrm{el}}(t)| \, \mathrm{d}t}{\int_{I_T} |P^{\varepsilon}_{\mathrm{el}}(t)| \, \mathrm{d}t}, \tag{49}$$

and

$$\Delta_{\mathrm{mc}} = \frac{\int_{I_T} |P^{\varepsilon}_{\mathrm{mc}}(t) - P_{\mathrm{mc}}(t)| \, \mathrm{d}t}{\int_{I_T} |P^{\varepsilon}_{\mathrm{mc}}(t)| \, \mathrm{d}t}. \tag{50}$$

Based on these results, MMM is able to capture well the non-linear and dynamic effects occurring in the composite material core even with only two harmonics for the macro-scale unknown fields. To visualize the results, Fig. 9 shows the electric and magnetic powers as a functions of time for both MHM and MMM. In the figure, macro-scale $\boldsymbol{A}$ and $\boldsymbol{T}$ have harmonics 1 and 3.

Table 6 compares MHM and MMM in the power quantities as a function of the number of elements in the homogenized composite material domain. For this comparison, harmonics 1 and 3 were used for $\boldsymbol{A}$ and $\boldsymbol{T}$. According to these results, the effect of the mesh density on the solution is small. Only with 2^3 elements in the homogenized domain, the values for the average powers are slightly higher. This result highlights the benefit of the homogenization method in MMM: it is possible to obtain accurate results even with larger macro-scale elements than the size of the cell.

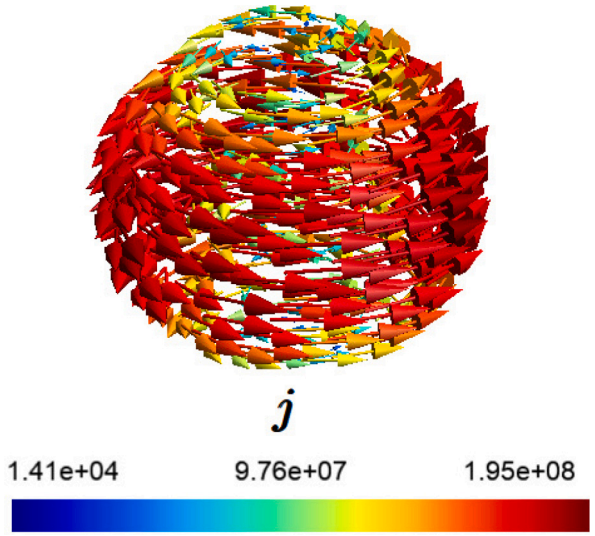

Fig. 7. Electric current density in the cell when sourced with y-directional $B(t) = 0.8 \cdot \sin(\omega t)$ [T] at the frequency of 100 kHz.

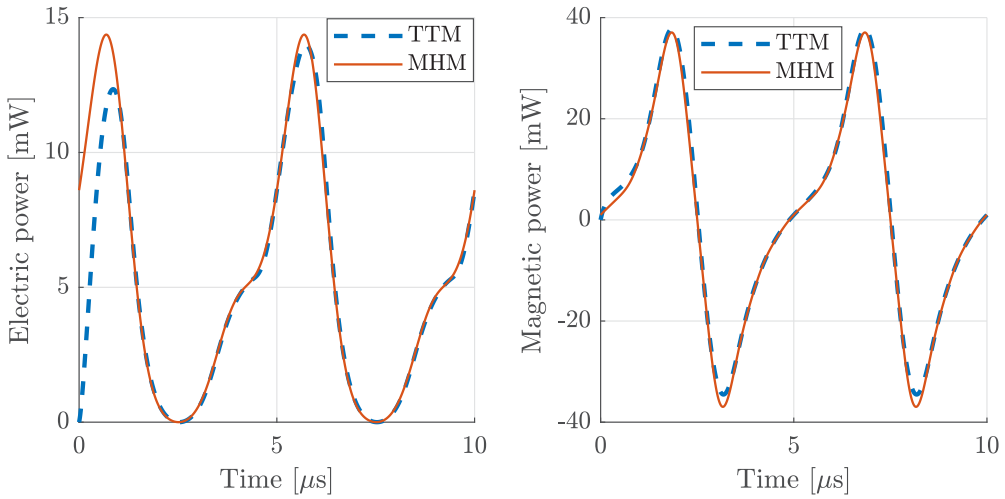

Fig. 8. Comparison between TTM and MHM in the electric (left) -and magnetic (right) power over the first period of excitation.

Table 6
The influence of the number of macro elements (#elems) in the CM-domain on the accuracy.

#elems in Ω_{CM}	2^3	3^3	4^3	5^3
Simulation time [min]	30	44	57	61
Number of CPUs	8	27	64	125
avg(P_{el}) [mW]	5.41	5.32	5.31	5.30
Δ_{el} [%]	2.51	1.67	1.72	1.69
avg($\lvert P_{mc} \rvert$) [mW]	17.69	17.12	17.22	17.15
Δ_{mc} [%]	7.02	4.83	5.01	4.85

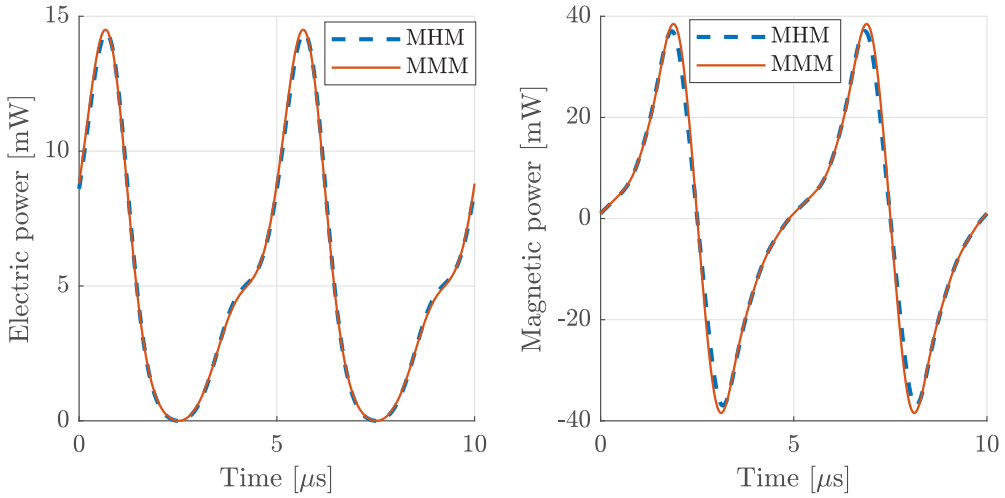

Fig. 9. Comparison between MHM and MMM in the electric (left) -and magnetic (right) power.

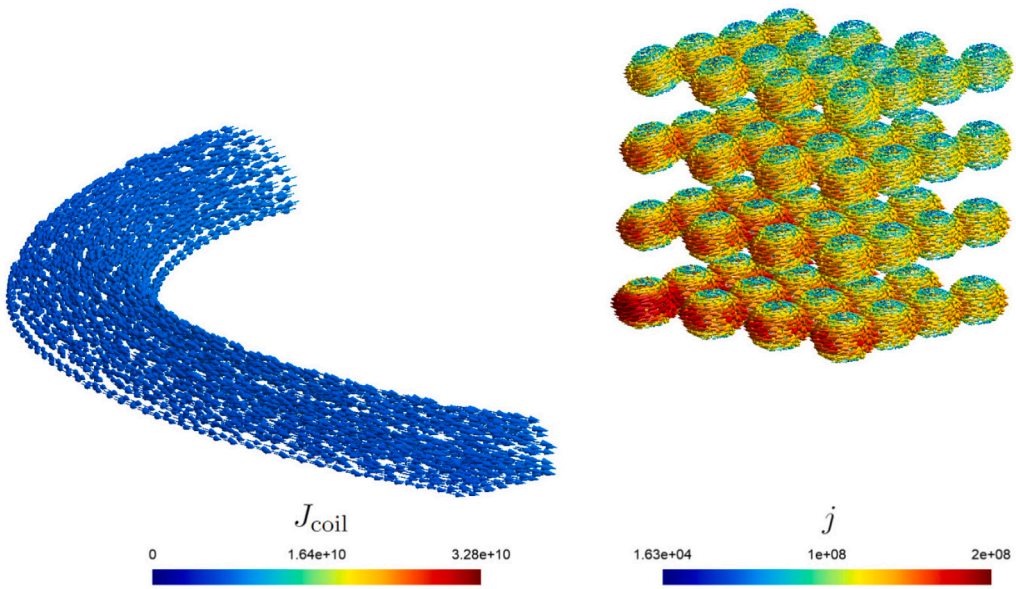

Fig. 10. In-time varying macroscale current density in the coil (left) induces eddy currents in the mesoscale particles (right). (For interpretation of the references to colour in this figure legend, the reader is referred to the web version of this article.)

Fig. 10 shows the macro-scale current density in the coil merged with the meso-scale induced currents in all the cells for 4^3 element discretization of the homogeneous CM domain. To visualize the magnetic flux density in the device, Fig. 11 shows $\boldsymbol{B}$ in the coil and the composite material domain (colour scale shown only in the composite domain). In addition, $\boldsymbol{b}$ is shown in the corner cell.

6. Conclusion

In this work, a modelling approach combining the multiharmonic method with the multiscale method was presented, where a $\boldsymbol{BJ}$-conforming magnetoquasistatic formulation was used. The developed approach was compared with the classical Galerkin finite-element method using TTM and MHM. The comparison was carried out by simulating a device made of a coil and a composite material core. The core was made of insulated, conducting and non-linearly magnetizing particles.

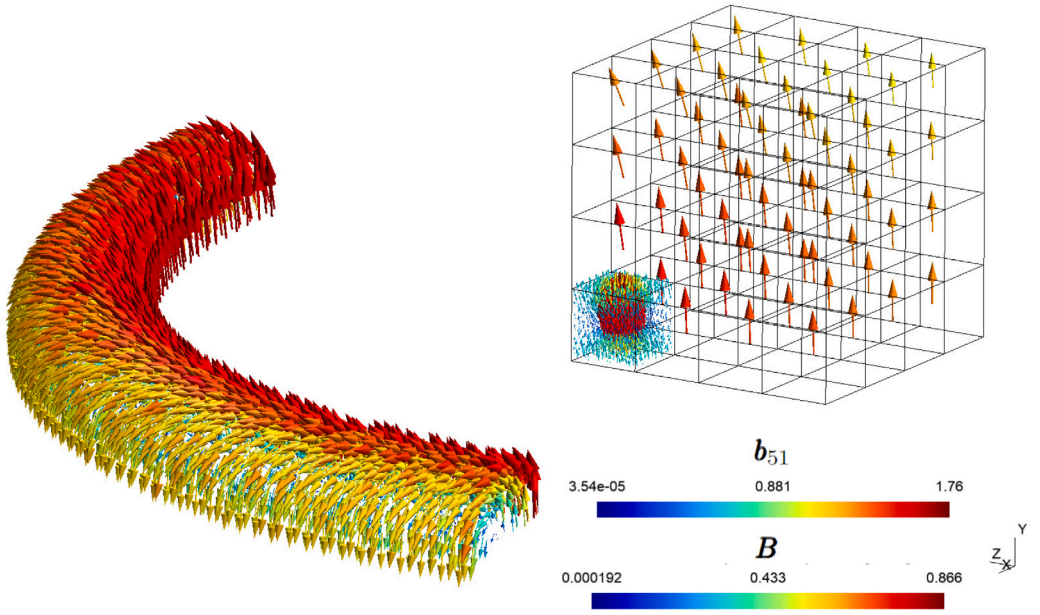

Fig. 11. Macroscale magnetic flux density in the coil and the composite material. In addition, mesoscale $\boldsymbol{b}$ is merged into the corner element of the homogenized core domain.

The developed multiharmonic multiscale method proved to be accurate and efficient at simulating the electromagnetic behaviour of magnetic composite materials in comparison to the classical approach. Using 4^3 elements in the homogenized composite material domain and two harmonics for the macro-scale unknown fields, the relative differences in the electric and magnetic powers were 1.73 % and 5.02 %, respectively. Using MMM, the simulation time was 1/53 of that of TTM, and 1/11 of that of MHM.

CRediT authorship contribution statement

Janne Ruuskanen: Writing – original draft, Validation, Supervision, Software, Methodology, Conceptualization. **Antoine Marteau:** Writing – review & editing, Methodology. **Innocent Niyonzima:** Writing – review & editing, Conceptualization. **Alexandre Halbach:** Software. **Joonas Vesa:** Writing – review & editing, Methodology, Conceptualization. **Gérard Meunier:** Writing – review & editing. **Timo Tarhasaari:** Writing – review & editing, Supervision. **Paavo Rasilo:** Writing – review & editing, Supervision.

Declaration of competing interest

The authors declare that they have no known competing financial interests or personal relationships that could have appeared to influence the work reported in this paper.

Data availability

No data was used for the research described in the article.

Acknowledgements

This project has received funding from the European Research Council (ERC) under the European Union's Horizon 2020 research and innovation programme (grant agreement No 848590). Academy of Finland (grant No 330062) and Ulla Tuominen foundation are also acknowledged for financial support.

Appendix. Homogenizing mesoscale fields

Here the derivations of the homogenized meso-scale quantities, the magnetic fields strength and the power density, are detailed.

A.1. Magnetic field strength

According to the Poynting's theorem, the total magnetoquasistatic electromagnetic power in the mesoscopic cell Ω_m is measured using the bilinear and reflexive Poynting's operator as

$$\mathcal{P}(\cdot,\cdot) = \int_{\Omega_\mathrm{m}} \mathrm{div}(\cdot \times \cdot)\, \mathrm{d}\Omega. \tag{A.1}$$

To derive the homogeneous macroscale quantities, let us require that the Poynting-measure equals over Ω_m for the macroscale $\boldsymbol{E}$ and $\boldsymbol{H}$ and for the mesoscale $\boldsymbol{e}$ and $\boldsymbol{h}$ as

$$\mathcal{P}(\boldsymbol{E},\boldsymbol{H}) = \mathcal{P}(\boldsymbol{e},\boldsymbol{h}) \tag{A.2}$$

Furthermore, the cell fields are decomposed into periodic and antiperiodic fields as

$$\boldsymbol{e} = \boldsymbol{E}_1 + \boldsymbol{e}_\mathrm{p} \tag{A.3}$$

$$\boldsymbol{h} = \boldsymbol{H}_1 + \boldsymbol{h}_\mathrm{p}, \tag{A.4}$$

where $\boldsymbol{e}_\mathrm{p}$, $\boldsymbol{h}_\mathrm{p}$ are cell periodic [7,20,21]. The macroscopic fields at a macrocale domain integration point are also decomposed as

$$\boldsymbol{E} = \boldsymbol{E}_1 + \boldsymbol{E}_0 \tag{A.5}$$

$$\boldsymbol{H} = \boldsymbol{H}_1 + \boldsymbol{H}_0, \tag{A.6}$$

where the fields $\boldsymbol{E}_0$, $\boldsymbol{H}_0$ are homogeneous, and the fields

$$\boldsymbol{E}_1 = -\partial_t \boldsymbol{B} \times \frac{\boldsymbol{x}}{2}, \tag{A.7}$$

$$\boldsymbol{H}_1 = \boldsymbol{J} \times \frac{\boldsymbol{x}}{2}, \tag{A.8}$$

produce the curl of $\boldsymbol{E}$ and $\boldsymbol{H}$ into the neighbourhood of the point of integration, where $\boldsymbol{x} = [x\ y\ z]^\mathrm{T}$. Measuring the curl of $\boldsymbol{E}$ and $\boldsymbol{H}$ in the cell gives the cell-homogenous fields $\partial_t \boldsymbol{B}$ and $\boldsymbol{J}$ as

$$\mathrm{curl}\ \boldsymbol{E} = -\partial_t \boldsymbol{B} \tag{A.9}$$

$$\mathrm{curl}\ \boldsymbol{H} = \boldsymbol{J}. \tag{A.10}$$

In this work, the cells do not carry any net-current since they are insulated — therefore $\boldsymbol{H}_1 = \boldsymbol{0}$. Furthermore, since $\boldsymbol{E}_0$ and $\boldsymbol{H}_0$ are cell-homogeneous, $\mathcal{P}(\boldsymbol{E}_0,\boldsymbol{H}_0) = 0$ and consequently

$$\mathcal{P}(\boldsymbol{E},\boldsymbol{H}) = \mathcal{P}(\boldsymbol{E}_1,\boldsymbol{H}_0). \tag{A.11}$$

Furthermore,

$$\mathcal{P}(\boldsymbol{e},\boldsymbol{h}) = \mathcal{P}(\boldsymbol{E}_1,\boldsymbol{h}_\mathrm{p}) \tag{A.12}$$

since for the periodic $\boldsymbol{e}_\mathrm{p}$ and $\boldsymbol{h}_\mathrm{p}$, $\mathcal{P}(\boldsymbol{e}_\mathrm{p},\boldsymbol{h}_\mathrm{p}) = 0$.

Now, due to the bilinearity of $\mathcal{P}$ and using the Gauss' theorem, the macroscopic $\boldsymbol{H}_0$ is derived based on (A.2), as

$$\begin{aligned}
&\mathcal{P}(\boldsymbol{E},\boldsymbol{H}) = \mathcal{P}(\boldsymbol{e},\boldsymbol{h}) \\
\Leftrightarrow &\mathcal{P}(\boldsymbol{E}_1,\boldsymbol{H}_0) = \mathcal{P}(\boldsymbol{E}_1,\boldsymbol{h}_\mathrm{p}) \\
\Leftrightarrow &\mathcal{P}(\boldsymbol{E}_1,\boldsymbol{H}_0 - \boldsymbol{h}_\mathrm{p}) = 0 \\
\Leftrightarrow &\int_{\Omega_\mathrm{m}} \mathrm{div}\left(\boldsymbol{E}_1 \times \left(\boldsymbol{H}_0 - \boldsymbol{h}_\mathrm{p}\right)\right)\, \mathrm{d}\Omega = 0 \\
\Leftrightarrow &\int_{\Gamma_\mathrm{m}} \boldsymbol{n} \cdot \left(\boldsymbol{E}_1 \times \left(\boldsymbol{H}_0 - \boldsymbol{h}_\mathrm{p}\right)\right)\, \mathrm{d}\Gamma = 0 \\
\Leftrightarrow &\int_{\Gamma_\mathrm{m}} \boldsymbol{E}_1 \cdot \left(\left(\boldsymbol{H}_0 - \boldsymbol{h}_\mathrm{p}\right) \times \boldsymbol{n}\right)\, \mathrm{d}\Gamma = 0,
\end{aligned} \tag{A.13}$$

where the boundary of Ω_m is

$$\Gamma_\mathrm{m}(x,y,z) = \Gamma_x^+ \cup \Gamma_x^- \cup \Gamma_y^+ \cup \Gamma_y^- \cup \Gamma_z^+ \cup \Gamma_z^-, \tag{A.14}$$

where

$$\Gamma_x^+ := \Gamma_\mathrm{m}(\frac{1}{2}d_\mathrm{meso}, y, z) \tag{A.15}$$

$$\Gamma_x^- := \Gamma_\mathrm{m}(-\frac{1}{2}d_\mathrm{meso}, y, z) \tag{A.16}$$

$$\Gamma_y^+ := \Gamma_\mathrm{m}(x, \frac{1}{2}d_\mathrm{meso}, z) \tag{A.17}$$

$$\Gamma_y^- := \Gamma_{\mathrm{m}}(x, -\frac{1}{2}d_{\mathrm{meso}}, z) \tag{A.18}$$

$$\Gamma_z^+ := \Gamma_{\mathrm{m}}(x, y, \frac{1}{2}d_{\mathrm{meso}}) \tag{A.19}$$

$$\Gamma_z^- := \Gamma_{\mathrm{m}}(x, y, -\frac{1}{2}d_{\mathrm{meso}}). \tag{A.20}$$

Since $\boldsymbol{h}_{\mathrm{p}}$ is periodic, i.e., $\boldsymbol{h}_{\mathrm{p}}(\Gamma_\cdot^+) = \boldsymbol{h}_{\mathrm{p}}(\Gamma_\cdot^-)$ for subscripts x, y and z, (A.13) yields for the homogeneous macroscale magnetic field strength the expression

$$\boldsymbol{H}_0 = \frac{1}{2d_{\mathrm{meso}}^2}\begin{bmatrix} \int_{\Gamma_y^+} h_x \,\mathrm{d}\Gamma + \int_{\Gamma_z^+} h_x \,\mathrm{d}\Gamma \\ \int_{\Gamma_x^+} h_y \,\mathrm{d}\Gamma + \int_{\Gamma_z^+} h_y \,\mathrm{d}\Gamma \\ \int_{\Gamma_x^+} h_z \,\mathrm{d}\Gamma + \int_{\Gamma_y^+} h_z \,\mathrm{d}\Gamma \end{bmatrix}, \tag{A.21}$$

where $h_j = \boldsymbol{h}_{\mathrm{p}} \cdot \hat{\boldsymbol{v}}_j$, and since $\boldsymbol{H}_1 = \boldsymbol{0}$, h_j also equals to $\boldsymbol{h} \cdot \hat{\boldsymbol{v}}_j$.

A.2. Power density

The homogenization of the cell power densities can be derived based on (A.2) as

$$\begin{aligned}
&\mathcal{P}(\boldsymbol{E}, \boldsymbol{H}) = \mathcal{P}(\boldsymbol{e}, \boldsymbol{h}) \\
\Leftrightarrow &\int_{\Omega_m} \mathrm{div}(\boldsymbol{E} \times \boldsymbol{H}) \,\mathrm{d}\Omega = \int_{\Omega_m} \mathrm{div}(\boldsymbol{e} \times \boldsymbol{h}) \,\mathrm{d}\Omega \\
\Leftrightarrow &\int_{\Omega_{\mathrm{m}}} \mathrm{curl}(\boldsymbol{E}) \cdot \boldsymbol{H} - \boldsymbol{E} \cdot \mathrm{curl}(\boldsymbol{H}) \,\mathrm{d}\Omega \\
&= \int_{\Omega_{\mathrm{m}}} \mathrm{curl}(\boldsymbol{e}) \cdot \boldsymbol{h} - \boldsymbol{e} \cdot \mathrm{curl}(\boldsymbol{h}) \,\mathrm{d}\Omega \\
\Leftrightarrow &\int_{\Omega_{\mathrm{m}}} \partial_t \boldsymbol{B} \cdot \boldsymbol{H} \,\mathrm{d}\Omega = \int_{\Omega_m} \partial_t \boldsymbol{b} \cdot \boldsymbol{h} + \boldsymbol{e} \cdot \boldsymbol{j} \,\mathrm{d}\Omega \\
\Leftrightarrow &|\Omega_{\mathrm{m}}| \partial_t \boldsymbol{B} \cdot \boldsymbol{H} = \int_{\Omega_{\mathrm{m}}} \partial_t \boldsymbol{b} \cdot \boldsymbol{h} + \boldsymbol{e} \cdot \boldsymbol{j} \,\mathrm{d}\Omega \\
\Leftrightarrow &\partial_t \boldsymbol{B} \cdot \boldsymbol{H} = \frac{1}{|\Omega_{\mathrm{m}}|} \int_{\Omega_{\mathrm{m}}} \partial_t \boldsymbol{b} \cdot \boldsymbol{h} \,\mathrm{d}\Omega + \frac{1}{|\Omega_{\mathrm{m}}|} \int_{\Omega_{\mathrm{mc}}} \boldsymbol{e} \cdot \boldsymbol{j} \,\mathrm{d}\Omega
\end{aligned} \tag{A.22}$$

where

$$p_{\mathrm{m}} = \frac{1}{|\Omega_{\mathrm{m}}|} \int_{\Omega_{\mathrm{m}}} \partial_t \boldsymbol{b} \cdot \boldsymbol{h} \,\mathrm{d}\Omega \tag{A.23}$$

is the macroscopic magnetic power density p_{m} that is the sum of the insulator domain (Ω_{mi}) power density

$$p_{\mathrm{mi}} = \frac{1}{|\Omega_{\mathrm{m}}|} \int_{\Omega_{\mathrm{mi}}} \partial_t \boldsymbol{b} \cdot \boldsymbol{h} \,\mathrm{d}\Omega \tag{A.24}$$

and of the conducting domain (Ω_{mc}) power density

$$p_{\mathrm{mc}} = \frac{1}{|\Omega_{\mathrm{m}}|} \int_{\Omega_{\mathrm{mc}}} \partial_t \boldsymbol{b} \cdot \boldsymbol{h} \,\mathrm{d}\Omega. \tag{A.25}$$

The term

$$p_{\mathrm{el}} = \frac{1}{|\Omega_{\mathrm{m}}|} \int_{\Omega_{\mathrm{mc}}} \boldsymbol{e} \cdot \boldsymbol{j} \,\mathrm{d}\Omega \tag{A.26}$$

is the macroscopic electric power density that consists of the eddy current losses only.

References

[1] H. Shokrollahi, K. Janghorban, Soft magnetic composite materials (SMCs), J. Mater Process. Technol. (ISSN: 0924-0136) 189 (1) (2007) 1–12.

[2] A. Bensoussan, J.-L. Lions, G. Papanicolaou, Asymptotic analysis for periodic structures, Vol. 374, American Mathematical Society, Rhode Island, 2011.

[3] Z. Yang, J. Cui, Y. Sun, J. Liang, Z. Yang, Multiscale analysis method for thermo-mechanical performance of periodic porous materials with interior surface radiation, Internat. J. Numer. Methods Engrg. 105 (5) (2016) 323–350.

[4] M.M. Ameen, R. Peerlings, M. Geers, A quantitative assessment of the scale separation limits of classical and higher-order asymptotic homogenization, Eur. J. Mech. A Solids 71 (2018) 89–100.

[5] Z. Yang, Y. Sun, Y. Liu, J. Cui, Prediction on nonlinear mechanical performance of random particulate composites by a statistical second-order reduced multiscale approach, Acta Mech. Sin. 37 (2021) 570–588.

[6] I. Niyonzima, Multiscale Finite Element Modeling of Nonlinear Quasistatic Electromagnetic Problems (Ph.D. thesis), FRIA - Fonds pour la Formation à la Recherche dans l'Industrie et dans l'Agriculture [BE], Uliège - Université de Liège, 2014.

[7] G. Meunier, V. Charmoille, C. Guerin, P. Labie, Y. Marechal, Homogenization for periodical electromagnetic structure: Which formulation? IEEE Trans. Magn. 46 (8) (2010) 3409–3412.

[8] I. Niyonzima, R.V. Sabariego, P. Dular, C. Geuzaine, Nonlinear computational homogenization method for the evaluation of eddy currents in soft magnetic composites, IEEE Trans. Magn. 50 (2) (2014) 61–64, http://dx.doi.org/10.1109/TMAG.2013.2286413.
[9] O. Bottauscio, V.C. Piat, M. Chiampi, M. Codegone, A. Manzin, Nonlinear homogenization technique for saturable soft magnetic composites, IEEE Trans. Magn. 44 (11) (2008) 2955–2958, http://dx.doi.org/10.1109/TMAG.2008.2001341.
[10] J. Ruuskanen, M. Lyly, A. Halbach, T. Tarhasaari, V. Lahtinen, T. Salmi, P. Rasilo, Modeling eddy current losses in HTS tapes using multiharmonic method, IEEE Trans. Appl. Supercond. 33 (5) (2023) 1–5, http://dx.doi.org/10.1109/TASC.2023.3242619.
[11] J. Dular, K. Berger, C. Geuzaine, B. Vanderheyden, What formulation should one choose for modeling a 3-D HTS motor pole with ferromagnetic materials? IEEE Trans. Magn. 58 (9) (2022) 1–4, http://dx.doi.org/10.1109/TMAG.2022.3167839.
[12] J. Gyselinck, P. Dular, C. Geuzaine, W. Legros, Harmonic-balance finite-element modeling of electromagnetic devices: a novel approach, IEEE Trans. Magn. 38 (2) (2002) 521–524, http://dx.doi.org/10.1109/20.996137.
[13] F. Bachinger, U. Langer, J. Schöberl, Numerical analysis of nonlinear multiharmonic eddy current problems, Numer. Math. 100 (2005) 593–616.
[14] A.K. Amert, V.V. Gozhenko, K.W. Whites, Calculation of effective material parameters by field averaging over lattices with non-negligible unit cell size, Appl. Phys. A 109 (2012) 1007–1013.
[15] J.C. Maxwell, A Treatise on Electricity and Magnetism, Vol. 1, Clarendon Press, 1873.
[16] F. Rapetti, F. Dubois, A. Bossavit, Discrete vector potentials for nonsimply connected three-dimensional domains, SIAM J. Numer. Anal. 41 (4) (2003) 1505–1527, http://dx.doi.org/10.1137/S0036142902412646.
[17] C. Geuzaine, J.-F. Remacle, Gmsh: A 3D finite element mesh generator with built-in pre- and post-processing facilities, Internat. J. Numer. Methods Engrg. 79 (11) (2009) 1309–1331, http://dx.doi.org/10.1002/nme.2579.
[18] N. Riva, A. Halbach, M. Lyly, C. Messe, J. Ruuskanen, V. Lahtinen, H-ϕ Formulation in sparselizard combined with domain decomposition methods for modeling superconducting tapes, stacks, and twisted wires, IEEE Trans. Appl. Supercond. 33 (5) (2023) 1–5, http://dx.doi.org/10.1109/TASC.2023.3240389.
[19] C. Lee, F. Reitich, M. Jolly, H. Banks, K. Ito, Piecewise linear model for field-responsive fluids, IEEE Trans. Magn. 37 (1) (2001) 558–560, http://dx.doi.org/10.1109/20.914377.
[20] M. El Feddi, Z. Ren, A. Razek, A. Bossavit, Homogenization technique for maxwell equations in periodic structures, IEEE Trans. Magn. 33 (2) (1997) 1382–1385, http://dx.doi.org/10.1109/20.582514.
[21] A. Marteau, I. Niyonzima, G. Meunier, J. Ruuskanen, N. Galopin, P. Rasilo, O. Chadebec, Magnetic field upscaling and B-conforming magnetoquasistatic multiscale formulation, IEEE Trans. Magn. 59 (5) (2023) 1–4, http://dx.doi.org/10.1109/TMAG.2023.3235208.